Neurobiology of Disease 115 (2018) 39–48

Contents lists available at ScienceDirect

Neurobiology of Disease

journal homepage: www.elsevier.com/locate/ynbdi

Translation-relevant EEG phenotypes in a mouse model of Fragile X Syndrome

Jonathan W. Lovelace[a], Iryna M. Ethell[b,c], Devin K. Binder[b,c], Khaleel A. Razak[a,b,*]

[a] Department of Psychology, University of California, Riverside, USA
[b] Neuroscience Graduate Program, University of California, Riverside, USA
[c] Division of Biomedical Sciences, School of Medicine, University of California, Riverside, USA

ARTICLE INFO

Keywords:
Fragile X Syndrome
Autism
Auditory cortex
Sensory hypersensitivity
Frontal cortex
EEG
Neural oscillations

ABSTRACT

Identification of comparable biomarkers in humans and validated animal models will facilitate pre-clinical to clinical therapeutic pipelines to treat neurodevelopmental disorders. Fragile X Syndrome (FXS) is a leading known genetic cause of intellectual disability with symptoms that include increased anxiety, social and sensory processing deficits. Recent EEG studies in humans with FXS have identified neural oscillation deficits that include enhanced resting state gamma power and reduced inter-trial coherence of sound evoked gamma oscillations. To determine if analogous phenotypes are present in an animal model of FXS, we recorded EEGs in awake, freely moving *Fmr1* knock out (KO) mice using similar stimuli as in the human studies. We report remarkably similar neural oscillation phenotypes in the *Fmr1* KO mouse including enhanced resting state gamma power and reduced evoked gamma synchronization. The gamma band inter-trial coherence of neural response was reduced in both auditory and frontal cortex of *Fmr1* KO mice stimulated with a sound whose envelope was modulated from 1 to 100 Hz, similar to that seen in humans with FXS. These deficits suggest a form of enhanced 'resting state noise' that interferes with the ability of the circuit to mount a synchronized response to sensory input, predicting specific sensory and cognitive deficits in FXS. The abnormal gamma oscillations are consistent with parvalbumin neuron and perineuronal net deficits seen in the *Fmr1* KO mouse auditory cortex indicating that the EEG biomarkers are not only clinically relevant, but could also be used to probe cellular and circuit mechanisms of sensory hypersensitivity in FXS.

1. Introduction

Fragile X Syndrome (FXS) is the most common genetic cause of intellectual disability with symptoms that overlap with autism spectrum disorders (ASD, Crawford et al., 2001). FXS is caused by a mutation in the *Fragile X Mental Retardation 1 (Fmr1)* gene and down-regulation of Fragile X Mental Retardation Protein (FMRP, Yu et al., 1991). FMRP is an RNA binding protein that regulates synaptic function through effects on protein translation (Darnell et al., 2011). Symptoms associated with FXS include increased anxiety, repetitive behaviors, social communication deficits, delayed language development and abnormal sensory processing (Wisniewski et al., 1991; Abbeduto and Hagerman, 1997; Miller et al., 1999; Musumeci et al., 1999; Roberts et al., 2001; Sabaratnam et al., 2001; Berry-Kravis, 2002; Hagerman and Hagerman, 2002; Hagerman et al., 2009; Van der Molen et al., 2010; Sinclair et al., 2017). Abnormal sensory processing in FXS includes hypersensitivity and reduced habituation to repeated sensory stimuli (Castren et al., 2003; Schneider et al., 2013). These symptoms that affect multiple sensory systems are seen early in development and may lead to increased anxiety and cognitive deficits.

Basic sensory processing mechanisms, in general, are more conserved across species compared to circuits shaping complex social and cognitive behaviors, providing an opportunity to better understand the pathophysiology of FXS/ASD at a neural circuit level. Auditory processing deficits are common in both humans with FXS (Castren et al., 2003; Schneider et al., 2013; Van der Molen and Van der Molen, 2013; Ethridge et al., 2016) and *Fmr1* knockout (KO) mice (Rotschafer and Razak, 2013, 2014; Lovelace et al., 2016; Wen et al., 2017), the mouse model of FXS (Bakker et al., 1994; Bernardet and Crusio, 2006). Recent EEG recordings from humans showed altered cortical oscillatory activity that may contribute to sensory hypersensitivity and social communication deficits in FXS (Ethridge et al., 2017; Wang et al., 2017). Gamma frequency power was enhanced in humans with FXS compared to healthy controls (Wang et al., 2017). The abnormal resting EEG power was correlated with social communication abnormalities in humans with FXS. When neural oscillations were induced with auditory

* Corresponding author at: Department of Psychology, University of California, 900 University Avenue, Riverside, CA 92521, USA.
E-mail address: Khaleel@ucr.edu (K.A. Razak).

https://doi.org/10.1016/j.nbd.2018.03.012
Received 22 November 2017; Received in revised form 16 February 2018; Accepted 28 March 2018
Available online 29 March 2018
0969-9961/

stimuli, inter-trial phase synchrony was reduced in humans with FXS, particularly at gamma frequencies (Ethridge et al., 2017). The non-phase locked single trial power was, however, enhanced in FXS. These results suggest that enhanced background gamma oscillations ('network noise') may contribute to hypersensitivity and interfere with stimulus-evoked synchronization in FXS. Importantly, these phenotypes were correlated with parent reports of social communication deficits and hypersensitive sensory responses suggesting clinical relevance of the EEG measures.

To understand the mechanisms of resting state and sound evoked oscillation deficits, it is necessary to identify analogous phenotypes in an animal model of FXS. We recently showed evidence for abnormal development of parvalbumin (PV) neurons and perineuronal nets (PNN) in the developing auditory cortex of *Fmr1* KO mice due to higher matrix metalloprotease-9 (MMP-9) activity (Wen et al., 2017). These deficits were correlated with enhanced spontaneous and sound-driven responses in *Fmr1* KO mice auditory cortex, which were normalized following genetic reduction of MMP-9 (Lovelace et al., 2016; Wen et al., 2017). PV neurons are critically involved in shaping gamma oscillations (Sohal et al., 2009), suggesting that abnormal gamma power may in fact be present in the auditory cortex of *Fmr1* KO mice.

Indeed, relative baseline gamma power in hippocampus/cortex is increased in *Fmr1* KO mice (Sinclair et al., 2017). Movement can alter neural responses in the visual cortex by increasing gain (Niell and Stryker, 2010; Dadarlat and Stryker, 2017). As *Fmr1* KO mice show hyperactivity (Bakker et al., 1994; Dansie et al., 2013; Sørensen et al., 2015), increased locomotion could contribute to the changes in spectral power composition of cortical EEGs observed in the *Fmr1* KO mice (Sinclair et al., 2017). However, it is unclear whether movement modulates auditory cortex responses in the *Fmr1* KO mice and if phase locking to auditory stimuli is abnormal in the *Fmr1* KO mouse cortex. To address these issues, we recorded resting and sound-evoked EEGs from the frontal and auditory cortex of adult, awake and freely moving *Fmr1* KO and WT mice. We compared resting EEG spectral power distribution during movement and non-movement (henceforth, 'still') by utilizing a piezoelectric sensor to detect movement. For auditory stimulation, we used paradigms analogous to those used in human studies (Ethridge et al., 2017). We report a number of novel EEG phenotypes in the *Fmr1* KO mice that are similar to those observed in humans and provide insights into abnormal sensory processing in FXS.

2. Methods

2.1. Mice

C57BL/6 *Fmr1* KO mice were obtained from Jackson Laboratories. All genotypes were confirmed by PCR analysis of genomic DNA isolated from mouse tails. Mice were maintained in an AAALAC accredited facility in 12 h light/dark cycles and fed standard mouse chow. All procedures were done according to NIH and Institutional Animal Care and Use Committee guidelines. Food and water was provided ad libitum. EEG recordings were obtained from 12 WT and 11 *Fmr1* KO mice, all males between 1.5 and 3 months of age.

2.2. Surgery

Mice were anesthetized with isoflurane inhalation (0.2–0.5%), and given an i.p. injection of ketamine and xylazine (K/X) (80/10 mg/kg). Mice were secured in a bite bar, and placed on a stereotaxic apparatus (model 930; Kopf, CA). Artificial tear gel was applied to the eyes to prevent drying. Toe pinch reflex was used to measure anesthetic state every 10 min throughout the surgery, and supplemental doses of K/X were administered as needed. Once the mouse was anesthetized, a midline sagittal incision was made along the scalp to expose the skull. A Foredom dental drill was used to drill 1 mm diameter holes in the skull overlying the right auditory cortex (−1.6 mm, +4.8 mm), left frontal lobe (+3.0 mm, −1.2 mm), and left occipital (−4.2 mm, −5.1 mm) (coordinate relative to Bregma: anterior/posterior, medial/lateral). Three channel electrode posts from Plastics One (MS333-2-A-SPC) were attached to 1 mm stainless steel screws from Plastics One (8L003905201F) and screws were advanced into drilled holes until secure, special care was taken not to advance the screws beyond the point of contact with the dura. Dental cement was applied around the screws, on the base of the post, and exposed skull. Triple antibiotic was applied along the edges of the dental cement followed by an injection of subcutaneous Buprenorphine (0.1 mg/kg). Mice were placed on a heating pad to aid recovery from anesthesia. A second Buprenorphine injection was administered between 6 and 10 h after surgery. Mice were then individually housed, returned to the vivarium and monitored daily until the day of EEG recordings. The separation between the last post-surgical Buprenorphine injection and EEG recordings was at least 3 days. The maximum number of days between surgery and EEG recordings was 5.

2.3. Acoustic stimulation

All experiments were conducted in a sound-attenuated chamber lined with anechoic foam (Gretch-Ken Industries, Oregon). Acoustic stimuli were generated using RPvds software and RZ6 hardware (Tucker Davis Technologies, FL) and presented through a free-field speaker (LCY-K100 ribbon tweeters; Madisound, WI) located 12 in. away directly above the cage. Sound pressure level (SPL) was modified using programmable attenuators in the RZ6 system. The speaker output was ~70 dB SPL at the floor of the recording chamber with fluctuation of +/− 3 dB for frequencies between 5 and 35 kHz as measured with a ¼ inch Bruel & Kjaer microphone.

We used acoustic stimulation paradigms that have been used in humans with FXS to enhance translation relevance. Ethridge et al. (2017) used a chirp-modulated tone (henceforth, 'chirp') to induce synchronized oscillations in their EEG recordings. The chirp is a tone or noise whose amplitude is modulated by a sinusoid whose frequency increases or decreases linearly in the 1–100 Hz range (Artieda et al., 2004; Purcell et al., 2004; Perez-Alcazar et al., 2008). The chirp facilitates a rapid measurement of transient oscillatory response (delta to gamma frequency range) to auditory stimuli of varying frequencies and can be used to compare oscillatory responses in different groups in clinical and pre-clinical settings (e.g., Purcell et al., 2004). Inter-trial coherence analysis (phase locking factor, Tallon-Baudry et al., 1996) can then be used to determine the ability of the neural generator to synchronize oscillations to the frequencies present in the stimulus. This is a variant of the auditory steady state or frequency following response, which can be measured separately at multiple modulation frequencies (Stapells, 2011). The chirp stimulus may be preferable over the traditional steady state stimulus in studies of children with neurodevelopmental disorders, as it can quickly and efficiently measure multiple modulation frequencies in a shorter period of time.

The chirp signal used was a 2 s broadband noise whose amplitude was modulated (100% modulation depth) by a sinusoid with increasing frequency (Up-Chirp from 1 to 100 Hz) or decreasing frequency (Down-Chirp from 100 to 1 Hz). To avoid onset responses contaminating phase locking to the amplitude modulation of the chirp, the stimulus was ramped in sound level from 0 to 100% over 1 s (rise time) which then smoothly transitioned into chirp modulation of the noise (see Fig. 5D). Up and Down chirp trains were presented 300 times each (for a total of 600 trains). Both directions of modulation were tested to ensure any frequency specific effects were not due to the frequency transition history within the stimulus. Up and Down trains were presented in an alternating sequence. The interval between each train was randomly varied between 1 and 1.5 s. In addition to the chirps, we also recorded ERPs with broadband noise to identify various components (P1, N1, P2) for comparison with human studies (Castren et al., 2003). After 5 min of EEG recording without any sound, ERPs were recorded in response to

trains of broadband noise. Each train consisted of 10 repetitions (0.25 Hz repetition rate) of the broadband noise. Each noise stimulus was 100 ms in duration, with a 5 ms rise/fall time. The inter-train interval was 8 s.

2.4. Electrophysiology

Resting and auditory ERP recordings were obtained using the BioPac system (BIOPAC Systems, Inc.) from awake and freely moving mice. Mice were allowed to habituate to the recording chamber for 15 min prior to being connected to the BioPac system. A three-channel tether was connected to the mouse's three-channel electrode post (implanted during surgery) under brief isoflurane anesthesia. The mouse was then placed inside a grounded Faraday cage after recovery from isoflurane. This tether was then connected to a commutator located directly above the cage. Mice were then allowed to habituate to being connected to the tether for an additional 15 min before EEG recordings were obtained.

The BioPac MP150 acquisition system was connected to two EEG 100C amplifier units (one for each channel) to which the commutator was attached, the lead to the occipital cortex was used as reference for both frontal and auditory cortex screw electrodes. The acquisition hardware was set to high-pass (> 0.5 Hz) and low-pass (< 100 Hz) filters. Normal EEG output data were collected with gain maintained the same (10,000×) between all recordings. Data were sampled at a rate of either 2.5 or 5 kHz using Acqknowledge software and down sampled to 1024 Hz post hoc using Analyzer 2.1 (Brain Vision Inc.). Sound delivery was synchronized with EEG recording using a TTL pulse to mark the onset of each sound in a train. 5 min of resting EEG was recorded in which no auditory stimuli were presented. This was followed by ERP recordings in response to trains of broadband noise, and Up and Down-Chirps. After these experiments were completed, mice were returned to the colony and perfused for histology at a later date.

2.5. Data analyses

Data were extracted from Acqknowledge and files saved in a file format compatible with BrainVision Analyzer 2.1 software. All data were notch filtered at 60 Hz to remove residual line frequency power from recordings. EEG artifacts were removed using a semi-automatic procedure in Analyzer 2.1 for all recordings. Less than 20% of data were rejected due to artifacts from any single mouse.

Resting (no auditory stimulus) EEG data were divided into 1 s segments and Fast Fourier Transforms (FFT) were run on each segment using 0.5 Hz bins and then average power ($\mu V/Hz^2$) was calculated for each mouse from 1 to 100 Hz. Power was then further binned into standard frequency bands: Delta (1-4 Hz), Theta (4-10 Hz), Alpha (10-13 Hz), Beta (13-30 Hz) and Gamma (30-100 Hz). Gamma was further divided into “Low Gamma” (30-55 Hz), and “High Gamma” (65-100 Hz). Chirp trains were analyzed using Morelet wavelet analysis. Chirp trains were segmented into windows of 500 ms before chirp onset to 500 ms after the end of the chirp sound (total of 3 s because each chirp was 2 s in duration). EEG traces were processed with Morelet wavelets from 1 to 100 Hz using power density ($\mu V/Hz$). Wavelets were run with a Morelet parameter of 10 as this gave the best frequency/power discrimination. This parameter was chosen since studies in humans found most robust difference around 40 Hz, where this parameter is centered (Ethridge et al., 2017). To measure phase synchronization at each frequency across trials, Phase Locking Factors (PLF) were calculated using wavelets across trials for each mouse (also referred to as Inter Trial Phase Coherence (ITPC)). In this report, PLF refers to ITPC. The equation used to calculate ITPC is:

$$ITPC(f,t) = \frac{1}{n}\sum_{k=1}^{n}\frac{F_k(f,t)}{|F_k(f,t)|}$$

where f is the frequency, t is the time point, and k is trial number. Thus, $F_k(f,t)$ refers to the complex wavelet coefficient at a given frequency and time for the kth trial. There were no < 275 trials (out of 300) for any given mouse after segments containing artifacts were rejected.

Single trial power (STP) was calculated by extracting absolute values from complex values obtained from the wavelet transformation (squareroot[$real^2$ + $imaginary^2$]) for each cell in each trial matrix. Absolute value matrices were then averaged for all trials for a given mouse, and group grand average matrices were then compiled for each group.

2.6. Statistical analysis and definition of movement states

Statistical group comparisons of chirp responses were quantified by wavelet power analysis. Analysis was conducted by binning time into 300 parts and frequency into 100 parts, resulting in a 100 × 300 matrix. t-tests (alpha = 0.05) were conducted for every cell in the matrix using Matlab, and cluster analysis was used for correcting for multiple comparisons. Cluster size was determined using Monte Carlo simulations resulting in cluster sizes of significance with at least 3 continuously adjacent cells along the y-axis on both sides, and 3 continuously adjacent cells along the x-axis on both sides (Maris and Oostenveld, 2007). In all cases where genotype means are reported, SEM was used. In all cases, p values < 0.05 were considered significant for ANOVA and Student's t-tests. Where t-tests were performed, r was calculated as an effect size. When interactions were found and multiple comparisons for ANOVA were made, data were analyzed on each factor for simple effects and corrected for using Bonferroni adjustments. If assumptions of sphericity were violated for repeated measures ANOVA, the Greenhouse-Geiser correction was used.

A piezoelectric transducer was placed underneath the recording cage to detect when the mouse was moving. The term ‘resting’ is used to indicate EEGs recorded in these mice without any specific auditory stimuli. The term ‘still’ is used to describe resting EEG when the mouse was stationary. The term ‘moving’ is used to describe resting EEG when the mouse was moving based on a threshold criterion for the piezoelectric signal that was confirmed by analyzing the video recording (under IR light) that was taken throughout the EEG recording procedure. The data were analyzed for 4 factors: Genotype (WT, *Fmr1* KO), Cortical region (auditory, frontal), Movement (moving, still), and Frequency (delta to gamma). We started analyzing the raw data using 4-way ANOVA, and further investigated differences by splitting the data and analyzing the factors separately as effects were revealed. Data are often expressed as ratio of WT values to gauge relative differences in various factors using the same scale.

3. Results

3.1. Fmr1 KO mice display increased Delta and Gamma resting EEG power

Resting EEG power was calculated in auditory and frontal cortex (AC and FC) of WT and KO mice by analyzing all frequency bands during movement and still states. Examples of one-second segments of resting EEG for each genotype, as well as genotype averages (+/− SEM) of power spectra are depicted in Fig. 1. Statistical analysis was performed with a four-way ANOVA: (Genotype × Region × Frequency × Movement) accounting for all factors during resting EEG. Main effects were observed for all factors: Genotype $F(1,420) = 21.59$, $p < 0.00001$, Region $F(1,420) = 26.8$, $p < 0.00001$, Frequency $F(4,420) = 221.87$, $p < 0.00001$, and Movement $F(1,420) = 43.37$, $p < 0.00001$. Interactions of note included Genotype X Frequency $F(4,420) = 13.65$, $p < 0.00001$, which indicates that specific frequency bands were affected in *Fmr1* KO mice, Genotype X Movement X Frequency $F(4,420) = 18.27$, $p < 0.00001$, which indicates that power was different between genotypes on specific frequency bands while the mice were either moving or still, but Genotype

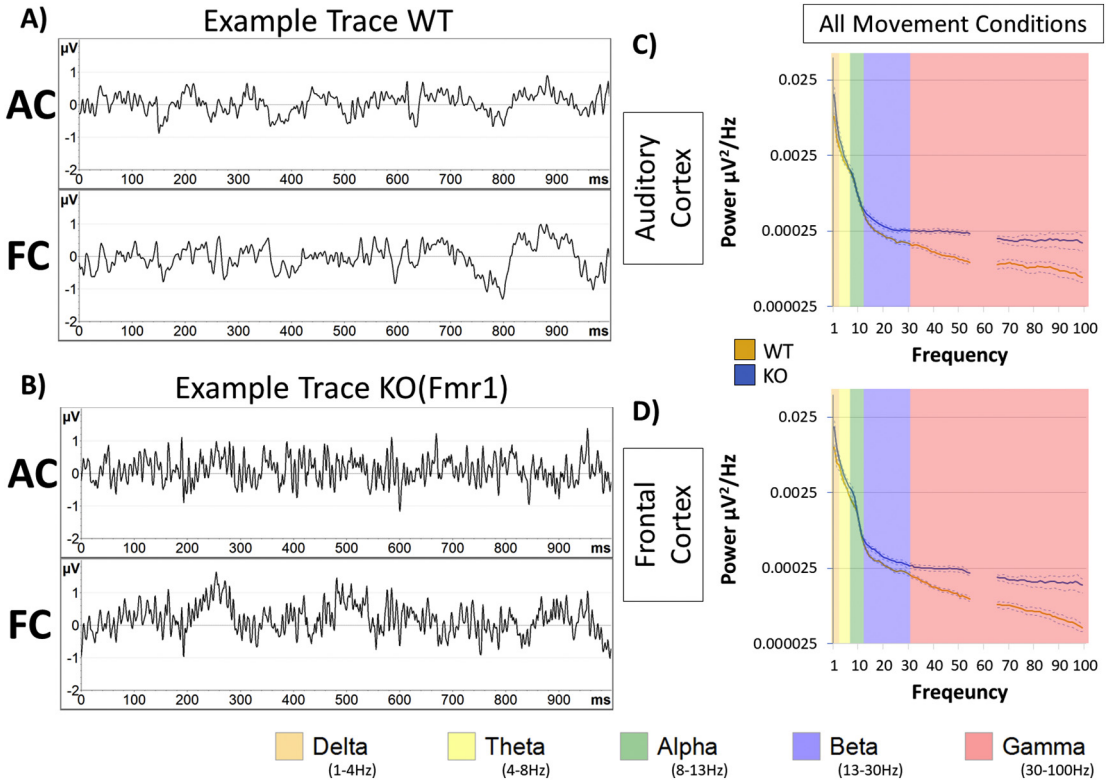

Fig. 1. Characterization of gamma power increase in *Fmr1* KO mice. Resting data (baseline, in the absence of auditory stimulation) was collected for 5 min and was divided into 1 s segments for spectral analysis. Depicted are examples segments from WT (A) and KO (B) which include simultaneous recording from Auditory Cortex (AC) and Frontal Cortex (FC). Power density (μV^2/Hz) was calculated for each artifact-free segment using Fast Fourier Transform, followed by averaging all segments for a given animal. These individual averages then contributed to the genotype grand average as seen in the AC (C) and FC (D) for each genotype. Obvious differences between genotype are observed at gamma frequencies (30–100 Hz in pink). Note: frequencies from 55 to 65 Hz were excluded in *all* analysis, as a 60 Hz notch filter was utilized to eliminate line noise.

X Region $F(1,420) = 0.41$, $p = 0.51905$ and Genotype X Region X Frequency $F(4,420) = 0.08$, $p = 0.98786$, were not significant, indicating that the power (of specific frequency bands) across regions was not different between genotypes.

Next, we determined which frequency bands were significantly different between WT and KO mice in different regions without considering movement as a factor. The data were split by region and a two-way ANOVA was run on Genotype X Frequency. To normalize data for each region and to determine relative changes in power across frequency bands, power values were expressed as a ratio of the KO to WT means (Fig. 2A–D). A ratio > 1 indicates more power in the KO mice. Two-way ANOVA (Genotype X Frequency) showed robust Bonferroni corrected post-hoc simple effects in the AC for Delta, $p = 0.00702$, Gamma, $p = 0.00014$, Low-Gamma, $p = 0.00177$ and High-Gamma, $p < 0.00001$ frequencies (Fig. 2B). The FC also showed similar differences for Delta, $p = 0.00853$, Gamma, $p = 0.00001$, Low-Gamma, $p = 0.00242$, and High-Gamma, $p < 0.00001$ frequencies (Fig. 2D).

3.2. Movement induces changes in power in both WT and KO

During the recording session, a piezoelectric sensor placed under the floor of the cage detected mouse movement in the recording arena (Fig. 3A). The percentage of time that mice spent moving during the recording period was not different between genotypes, $t(21) = 0.614$, $p = 0.546$, $r = 0.1328$ (Fig. 3B), indicating that the genotype spectral differences were not due to differences in activity as gauged by movement. Nevertheless, we analyzed EEG during movement and still states to determine if locomotion induced differences in EEG signal in AC and FC. Ratio of the power during movement and still state was calculated for each frequency band and region (Figs. 3C & 2F). Repeated Measures ANOVA (move/still) was then run for each genotype and each region separately. For the AC of WT animals, there were main effects of Movement $F(1,11) = 24.651$, $p < 0.00001$, Frequency $F(2.06, 22.63) = 6.629$, $p = 0.00512$, and Movement X Frequency $F(2.12, 23.32) = 11.125$, $p = 0.00034$. Simple effects were present in the AC of WT in all frequency bands: Delta, $p = 0.01534$, Theta, $p = 0.00420$, Alpha, $p = 0.01422$, Beta, $p = 0.03903$, Gamma, $p = 0.00009$, Low-Gamma, $p = 0.00002$, High-Gamma, $p = 0.00076$ (Fig. 3D). The FC of WT animals displayed similar effects: Movement $F(1,11) = 29.486$, $p = 0.00021$, Frequency $F(1.76, 19.34) = 7.601$, $p < 0.00001$, and Movement X Frequency $F(2.38, 26.18) = 19.227$, $p < 0.00001$, and simple effects: Theta, $p = 0.00016$, Alpha, $p = 0.00051$, Gamma, $p < 0.00001$, Low-Gamma, $p = 0.00002$, High-Gamma, $p = 0.00001$ (Fig. 3G).

For the AC of KO animals, there were main effects of Movement $F(1,10) = 49.529$, $p = 0.00004$, Frequency $F(1.64, 16.43) = 11.932$, $p = 0.00104$, and Movement X Frequency $F(1.33, 13.29) = 14.135$, $p = 0.00128$. Repeated measure simple effects were also present in all frequency bands: Delta, $p = 0.00086$, Theta, $p = 0.02458$, Alpha, $p = 0.00425$, Beta, $p = 0.00039$, Gamma, $p = 0.00003$, Low-Gamma, $p < 0.00001$, High-Gamma, $p = 0.00036$ (Fig. 3E). The FC of KO animals displayed similar effects: Movement $F(1,10) = 51.808$, $p = 0.00003$, Frequency $F(1.49, 14.89) = 5.447$, $p = 0.02348$, and Movement X Frequency $F(2.08, 20.81) = 8.475$, $p = 0.00184$, and repeated measure simple effects: Delta, $p = 0.01587$, Theta, $p = 0.00861$, Alpha, $p = 0.00014$, Beta, $p = 0.00042$, Gamma, $p = 0.00005$, Low-Gamma, $p < 0.00001$, High-Gamma, $p = 0.00034$ (Fig. 3H). In general, we observed an increase in power in both WT and KO mice across all frequency bands and regions when animals were moving. The few exceptions were limited to no change in WT Delta and Beta power while

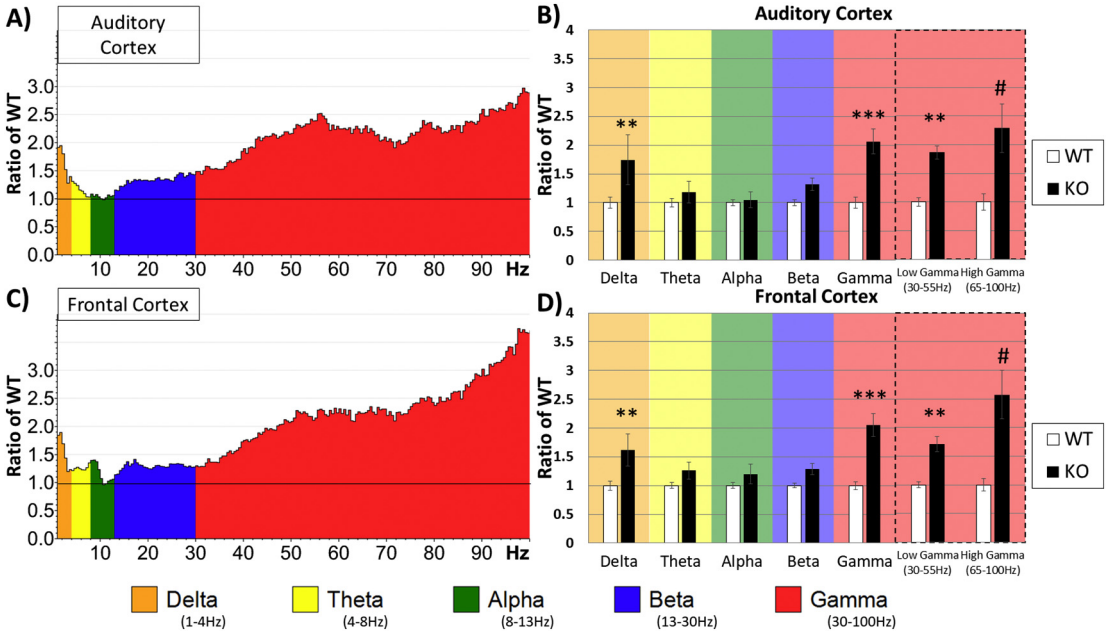

Fig. 2. Increased resting state gamma and delta power in F*mr1* KO mice. Five minutes of resting (non-stimulus) EEG data from electrodes implanted in the auditory cortex (A, B) and frontal cortex (C, D) of WT and KO animals was recorded and FFT analysis was done to determine spectral power. Average power in the *Fmr1* KO mouse auditory cortex (A) and frontal cortex (C) is expressed as the ratio of WT levels. A value of 1 (horizontal black line) indicates no mean difference in power at that frequency between WT and KO while values above the black line indicate KO > WT, and below KO < WT. Auditory (B) and frontal (D) cortex values were divided into standard frequency bands and post-hoc simple effects after two-way ANOVA revealed differences in delta and gamma frequency ranges. The gamma band was further subdivided into low and high gamma revealing genotype differences in both bands. Both cortical regions show significant increase in delta and gamma ranges in *Fmr1* KO mice. $*p < 0.05$, $**p < 0.01$, $***p < 0.001$, $****p < 0.0001$, $\#p < 0.00001$.

Theta in both AC and FC of WT mice was decreased.

3.3. Increased delta power in Fmr 1 KO mice is related to movement

Finally, comparisons between genotypes were conducted as in Fig. 2, except data were split based on movement. To normalize data for each region and to determine relative changes in power across frequency bands, power values in KO mice were expressed as a ratio of KO to WT means (Fig. 4). Two-way ANOVA of Genotype X Frequency was conducted for each region and movement state. When the mouse was

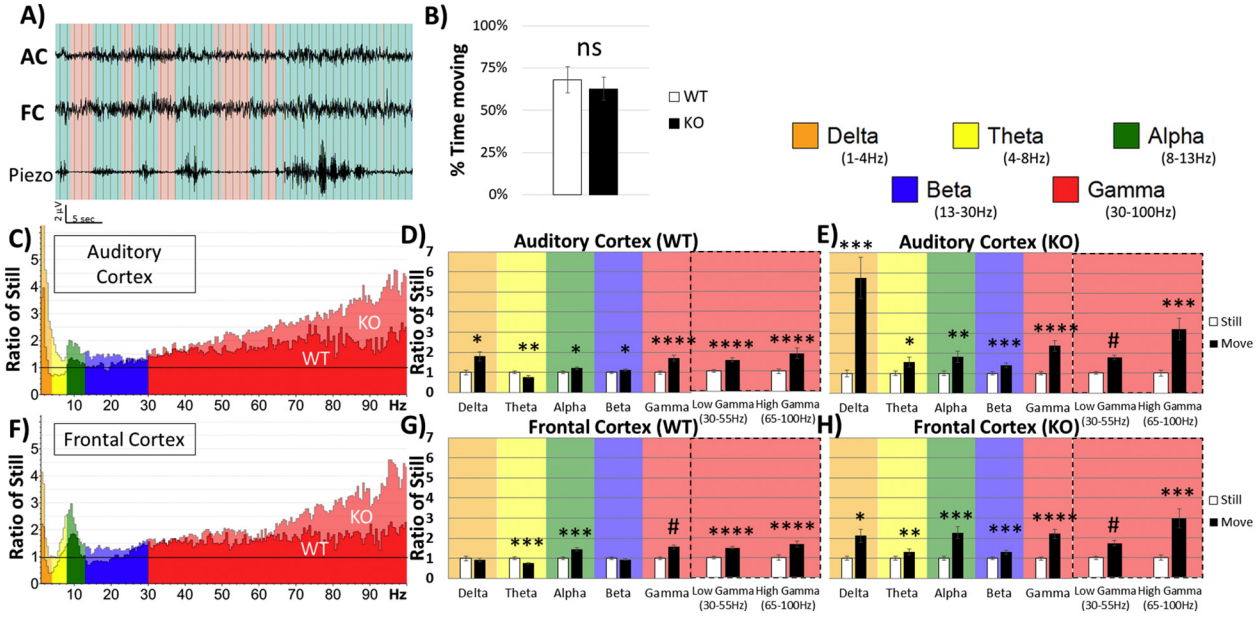

Fig. 3. Movement affects spectral EEG power in the auditory and frontal Cortex. (A) A Piezo-electric transducer was placed under the floor of the recording chamber while resting EEG was collected. Data were then divided into movement (blue) and still (red) states, based on threshold crossing on the Piezo channel. (B) Total time spent moving or still during the resting (non-stimulus) EEG recordings was calculated for each mouse. No significant differences between WT and KO mice were observed in the time moving. Auditory cortex (C) and frontal cortex (F) values represent power during movement divided by the power while still. This allows for within subject analysis of movement state on power for each group. (D) Repeated Measures (still-white and moving-black) separated into frequency bands in AC of WT, (E) AC of KO, (G) FC of WT, and (H) FC of KO. A general increase in power was present during movement in both AC and FC in both genotypes, but as seen in (C) and (F), the increase in *Fmr1* KO mice was much larger. $*p < 0.05$, $**p < 0.01$, $***p < 0.001$, $****p < 0.0001$, $\#p < 0.00001$.

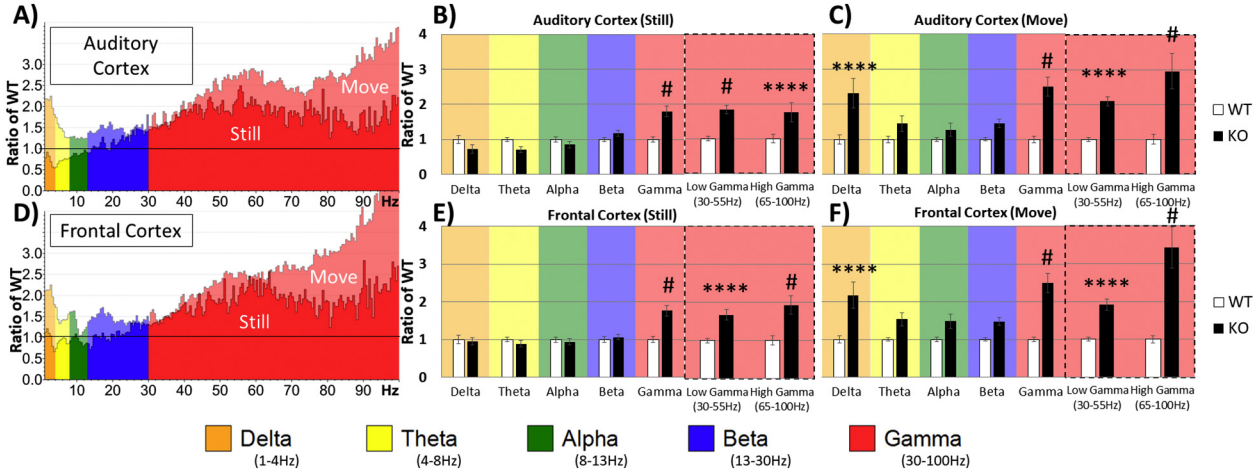

Fig. 4. Differences in Power between WT and *Fmr1* KO depend on movement state. (A&D) Same data as in Fig. 2 (A&C), but further divided by movement state. In both AC and FC, gamma band power was enhanced in *Fmr1* KO relative to WT regardless of movement state. However, the delta power increase in *Fmr1* KO was seen only when the mice were moving. Quantification of these observations is shown in the plots to the right. (B) When the mice were still, significantly increased gamma power is seen in AC of KO mice. (C) When the mice were moving, both gamma and delta power were increased in KO mice. (E, F) Essentially identical effects of movements on power across various EEG frequencies were also observed in the frontal cortex (FC). *$p < 0.05$, **$p < 0.01$, ***$p < 0.001$, ****$p < 0.0001$, #$p < 0.00001$.

still, the AC showed robust Bonferroni corrected post-hoc simple effects on Gamma, $p < 0.00001$, Low-Gamma, $p < 0.00001$, and High-Gamma, $p = 0.00001$ (Fig. 4B). The FC during still state also showed similar differences on Gamma, $p < 0.00001$, Low-Gamma, $p = 0.00003$, and High-Gamma, $p < 0.00001$ (Fig. 4E). However, during movement the AC showed differences in Delta, $p = 0.00002$, in addition to Gamma, $p < 0.00001$, Low-Gamma, $p = 0.00040$, and High-Gamma, $p < 0.00001$ (Fig. 4C). The FC during movement was similar to AC: Delta, $p = 0.00006$, Gamma, $p < 0.00001$, Low-Gamma, $p = 0.00158$, and High-Gamma, $p < 0.00001$ (Fig. 4F).

Repeated measures analysis (Movement × Frequency) of KO power relative to WT (comparing KO values of Fig. 4B to C, and also Fig. 4 E to F) revealed movement induced changes in power that are augmented in KO in all frequency bands and in both regions (all post hoc simple effects $p < 0.05$). The largest mean differences between still and movement states in AC were in Delta (mean difference = 1.591, $p = 0.00299$) and High Gamma (mean difference = 1.205, $p = 0.002$) and in FC, Delta (mean difference = 1.223, $p = 0.01089$) and High Gamma (mean difference = 1.497, $p = 0.00182$). Thus, power was enhanced in KO animals during movement state in all frequency bands compared to WT, but the frequency bands that were most sensitive were Delta and High Gamma (Fig. 4).

3.4. Gamma synchronization is reduced in Fmr1 KO mice

As the resting gamma band power was increased in the *Fmr1* KO mouse cortex, we hypothesized that this increased baseline gamma would lead to a deficit in mounting a specific gamma frequency-locked response to sounds. Both up and down chirps were tested to ensure that the differences are specific to modulation frequencies and are not affected by the direction of frequency change in the sound. After repeated chirp presentation (300 trials for up, 300 for down), the phase locking factor (PLF) was calculated across trials in the time by frequency domain using Morlet Wavelet analysis. We found increased EEG oscillations that matched the frequency of the chirp and were seen as increased PLF along a diagonal, from 0 to 2 s and 1–100 Hz. After grand average PLF was calculated for each group (Fig. 5 A and B), WT means were subtracted from *Fmr1* KO means (Fig. 5C). We observed reduced PLFs along the diagonal of the chirp in both the AC and FC of *Fmr1* KO mice (depicted in blue, Fig. 5A, B, and C). For statistical analysis, clusters of *p*-values were calculated and these differences are overlaid on the chirp response to demonstrate quantitative differences between each genotype after correction for multiple comparisons (Fig. 5C). In AC, statistical differences between genotypes are in two main clusters which span from Beta to Low-Gamma (~13–50 Hz) and in High-Gamma (~70–100 Hz), whereas PLFs are significantly reduced in the FC across the entire gamma range (~30–100 Hz). Similar patterns and statistics of PLF were observed for both up and down chirps (data not shown).

3.5. Increased non-phase locked single trial power in KO mice during chirp stimulation

Additionally, we investigated non-phase locked Single Trial Power (STP) during the chirp stimulation period (Fig. 6). Using the same statistical cluster analysis as for chirp, the *Fmr1* KO mice showed an increase in background gamma power in both the AC and FC in frequency bands between ~25 and 100 Hz (Fig. 6C). The increased non-phase locked power occurring in the background could contribute to the PLF deficit observed in Fig. 5. We also investigated STP in the silence between chirps, and the differences in non-phase locked STP were the same as during the Chirp (data not shown).

3.6. Fmr1 KO mice display increased amplitude and delayed latencies of sound evoked ERPs

Previous studies in humans with FXS showed enhanced amplitudes of ERP N1 and P2 components (Castren et al., 2003; Van der Molen and Van der Molen, 2013). To determine whether similar phenotypes are present in the *Fmr1* KO mice, we calculated the amplitudes and latencies of P1, N1 and P2 components of the ERP (Fig. 7). The amplitudes of P1 and P2 were not significantly different across genotypes in either AC or FC, although there was a trend for larger P1 amplitude in AC $t(21) = -1.902$, $p = 0.07096$, $r = 0.38$, and FC $t(21) = -1.632$, $p = 0.11749$, $r = 0.33$ (Fig. 7C). For N1, the amplitude was significantly higher in the FC, $t(21) = 2.094$, $p = 0.04848$, $r = 0.41$, with a non-significant trend in the AC, $t(21) = 1.945$, $p = 0.06519$, $r = 0.39$ (Fig. 7E). In the AC, both P1, $t(21) = -2.175$, $p = 0.04117$, $r = 0.42$ (Fig. 7D), and N1, $t(21) = -4.455$, $p = 0.00022$, $r = 0.69$ (Fig. 7F), latencies were significantly longer in KO compared to WT, while in the FC only the P1 latency was significantly longer, $t(21) = -2.37$, $p = 0.02742$, $r = 0.45$ (Fig. 7D). There was no difference in P2 latencies in either AC or FC.

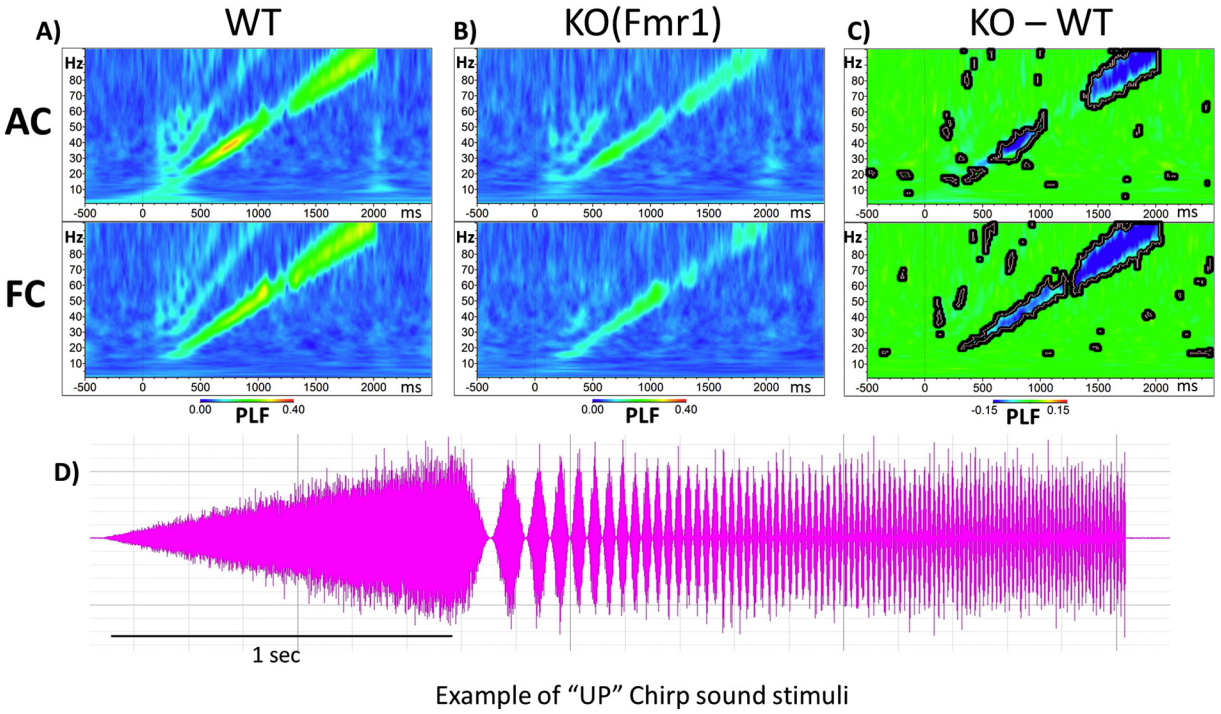

Fig. 5. *Fmr1* KO mice are deficient in Phase Locking to Auditory "Up Chirp" stimuli. (A, top row) Grand average WT Phase Locking Factor (PLF) to upward chirp in auditory cortex (AC). (A, bottom row) PLF in the frontal cortex (FC). Increased phase locking along the diagonal matches the modulation frequency of the chirp in both AC and FC. (B, top row) Auditory cortex grand average PLF to up chirp in KO mice. (B, bottom row) Grand average PLF in FC of KO mice. It can be seen that in both AC and FC, the PLF values are reduced in KO compared to WT mice. (C, top row) Auditory cortex WT PLF values are subtracted from KO values with blue areas indicating KO < WT, green areas no difference, and red KO > WT. Statistical cluster analysis reveals time x frequency bands that are significantly different between groups highlighted by bolded black borders. (D) Example "Up Chirp" auditory stimuli.

3.7. Analyses of similarity between AC and FC EEG signals

Because EEG signals were recorded simultaneously from the AC and FC, and the general results in terms of genotype differences were similar between the two regions, we examined the extent to which volume conduction may influence signals recorded at AC and FC. To determine the extent of similarity between the two channels (and the effect of volume conduction), two measures of phase synchronization were calculated between the two channels. We included all animals from both genotypes (n = 23). Phase locking value (PLV) was calculated as described by Lachaux et al. (1999). PLV between the two channels revealed a high synchronization index across all frequency bands (~0.73). PLV is sensitive to effects of volume conduction, so for comparison, we also calculated weighted phase lag index (WPLI) as described by Vinck et al. (2011). This measure is less sensitive to volume conduction. WPLI across all frequency bands between AC and FC was relatively low (~0.10). The high PLV and the low WPLI together indicate that the raw signals from FC and AC contained at least some overlapping information possibly due to volume conduction. Similar results and analysis have also been reported in rat EEG using electrode

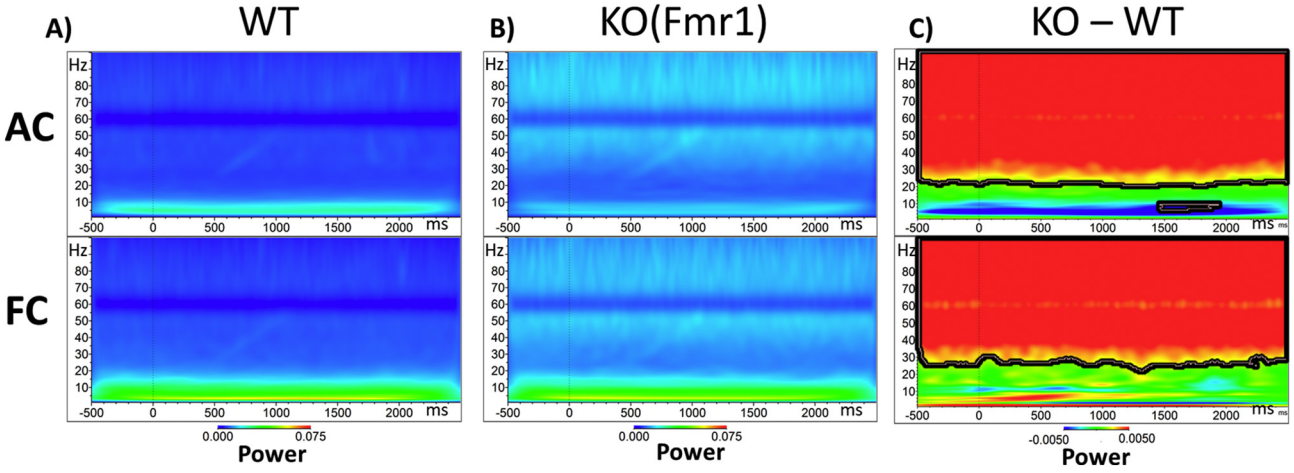

Fig. 6. Single Trial Power (STP) of *Fmr1* KO mice is increased in the Gamma Range during Chirp Stimulation. (A) Grand average WT STP to up chirp in auditory cortex (AC, top row) and frontal cortex (FC, bottom row). This is on-going 'background' power during auditory stimulation B) AC (top) and FC (bottom) grand average KO STP to up chirp. C) AC (top) and FC (bottom) STP values from WT are subtracted from KO values. Blue areas indicating KO < WT, green areas no difference, and red KO > WT. Statistical cluster analysis reveals time x frequency bands that are significantly different between groups highlighted with bolded black borders.

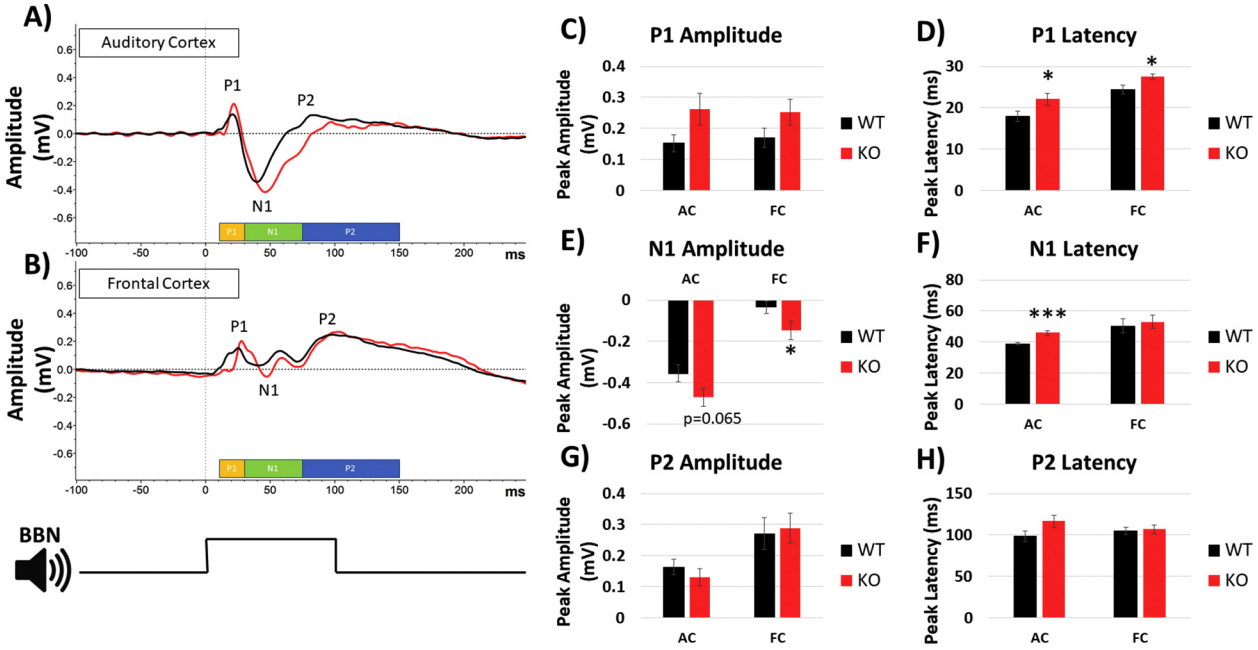

Fig. 7. ERP in response to broadband noise in auditory and frontal cortices. Broad Band Noise (BBN) with 100 ms duration was played to mice at a rate of 0.25 Hz for 1000 repetitions. (A) Grand average ERPs compiled from all mice in each group from the AC and (B) FC. Peaks were determined by pre-defined time windows displayed at the bottom: P1 (yellow, 10-30 ms), N1 (green, 30-75 ms), and P2 (blue, 75-150 ms). (C) No difference was detected in P1 amplitude, but (D) P1 latency was significantly longer in KO mice in both AC and FC. E) N1 amplitude was significantly larger in the FC of the KO mice with a trend towards increase in AC ($p = 0.065$). (F) N1 latency was significantly longer in AC, but no differences were seen in the FC. (G-H) Neither P2 amplitude nor latencies showed genotype differences in AC or FC. $*p < 0.05$, $**p < 0.01$, $***p < 0.001$, $****p < 0.0001$, $\#p < 0.00001$.

arrays and screw electrodes with the same conclusion (Stienen et al., 2016). However, it is also apparent that the AC and FC sites contain independent sources of information. Thus, similarities in AC and FC should not solely be considered artifacts of volume conduction between sites, but rather both AC and FC exhibit similar differences between genotypes. Future studies can investigate if FC and AC EEG signals respond differently to therapeutics and/or genetic manipulations using the same recording set up.

4. Discussion

The first main finding of this study is that resting state delta (1–4 Hz) and gamma (30–100 Hz) power is increased in both the auditory and frontal cortex of *Fmr1* KO mice compared to WT mice. The enhanced resting gamma power is consistent with a previous study on *Fmr1* KO mice (Sinclair et al., 2017). Additionally, we show that the enhanced gamma power in *Fmr1* KO mice compared to WT mice is independent of movement state. Although power at various frequency bands increased with movement in both WT and *Fmr1* KO cortex, there was a larger increase in KO mice (in delta and gamma band power) compared to WT. Second, the ability of cortex to produce synchronous stimulus-induced oscillations was reduced in *Fmr1* KO mice, which was most apparent at gamma frequencies. Third, *Fmr1* KO cortex showed enhanced non-phase locked single trial power following chirp stimulus. Finally, we also observed longer latency and increased amplitude of ERP components. The mouse ERPs are consistent with human FXS data in terms of increased N1 amplitude (Castren et al., 2003; Van der Molen et al., 2012a, 2012b). However, unlike in humans (Van der Molen et al., 2012a, 2012b), P2 amplitude augmentation was not seen in the mouse. The longer latency of N1 has been observed in autism spectrum disorder (using MEG, Gage et al., 2003), but not in FXS (Van der Molen et al., 2012a, 2012b). Except for the two exceptions noted above, the mouse data are remarkably similar to those reported in humans with FXS and suggest enhanced 'background noise' in AC and FC with a concomitant deficit in the ability of cortical neural generators to produce temporally precise responses (Ethridge et al., 2017; Wang et al., 2017). These data are also consistent with observations that auditory information processing is impaired in FXS (Van der Molen et al., 2012b). The similarity in EEG measures between humans and mice indicate that EEG/ERP recordings can serve as objective, physiological probes that serve as surrogate biomarkers to develop therapeutics to treat symptoms of FXS (Schneider et al., 2013; Sinclair et al., 2017).

Analyzing the EEG data according to whether the mouse was still or moving provides additional insights into the resting state neural oscillations. Even in the WT mice, movement was associated with enhanced gamma in both auditory and frontal cortex. The enhanced gamma in AC during movement indicates that basic sensory processing may be altered when an animal is moving. These data are consistent with findings in visual cortex that showed that locomotion increased the gain of visual cortex neurons (Niell and Stryker, 2010), improved encoding of visual stimuli (Dadarlat and Stryker, 2017) and suggest that locomotion may also affect auditory processing. However, regardless of whether the mouse was moving or not, low and high gamma power were more enhanced in the auditory cortex of *Fmr1* KO mice relative to WT mice. Our data are also consistent with observations in the visual cortex of a rat model of FXS wherein increased gamma activity was seen regardless of whether the rat was moving or was in 'quiet rest' state (Berzhanskaya et al., 2017). In contrast, enhanced delta power was seen in KO relative to WT mice only when the mice were moving. Taken together, these data indicate that resting gamma abnormalities in *Fmr1* KO mice (Sinclair et al., 2017; this study) are likely not a result of enhanced movement.

The EEG data observed in the mouse are consistent with findings in humans with FXS, and more broadly with ASD (Orekhova et al., 2007; Wang et al., 2013; Sinclair et al., 2016). Wang et al. (2013) suggested that children with ASD show an abnormal 'U' shaped profile of power spectrum of resting EEG with enhanced low-frequency (delta) and high-frequency (beta/gamma) power. Our data in the *Fmr1* KO mice also show a 'U' shaped power spectrum, due to abnormally enhanced delta and gamma power. A decrease in theta/alpha power was not present.

Ethridge et al. (2017) and Wang et al. (2017) reported enhanced resting gamma power, reduced chirp-evoked phase locking in gamma frequencies and enhanced non-phase locked single trial power in humans with FXS. The enhanced resting state gamma frequency power and non-stimulus locked single trial power in gamma frequency band were correlated with clinically relevant measures including heightened sensory sensitivity and autism-associated social impairment (Social Communication Questionnaire). Although enhanced delta power was not observed in humans, this might be due to the fact that the subjects were seated and watching a silent video. Our data also show no difference in delta power when the mice were not moving (Fig. 4). Low frequency abnormalities were nevertheless found in humans with FXS with enhanced theta band power relative to healthy controls (Van der Molen and Van der Molen, 2013, Wang et al., 2017). These similarities in EEG measures between humans and mice suggest the importance of studying basic sensory processing using analogous experimental design and approach in generating translation-relevant biomarkers. These measures may be useful outcome measures in the preclinical to clinical drug development pipeline and can be also employed in stratification of patient population for appropriate treatment strategies using a combination of EEGs and pharmacology (Berry-Kravis et al., 2018). In particular, the finding that a particular drug candidate has robust effects on normalizing EEG parameters such as resting gamma power and phase-locked synchronization in both humans and mice would enable targeting and correlation of those drugs with clinical parameters.

Previous studies in the adult *Fmr1* KO mice auditory cortex showed enhanced responses to tones and broader frequency tuning of single neurons (Rotschafer and Razak, 2013). In addition, there is reduced habituation of ERPs to repeated sounds in *Fmr1* KO mice as compared to WT mice (Lovelace et al., 2016). Together these data indicate that for any sound, more neurons will respond with a greater response magnitude over a sustained period. The enhanced ERP amplitude is consistent with this interpretation. The present data provide evidence that background network noise and non-phase locked single trial power are also higher in the AC of *Fmr1* KO mice. This abnormal milieu of baseline and evoked responses is likely to underlie hypersensitivity in humans with FXS. Perhaps the system is forced to produce a larger response to obtain sufficient signal to noise ratios under normal processing conditions. The inability of the system to synchronize responses to a modulated sound stimulus, particularly in the gamma range, may also be related to the enhanced background activity. Gamma band activity is involved in a broad array of sensory and cognitive processes, several of which are affected in FXS. The gamma phase-locking deficits may cause sensory discrimination deficits (Cardin et al., 2009; Salinas and Sejnowski, 2001; Sohal et al., 2009) that may lead to delayed language and cognitive development in FXS (Abbeduto et al., 2007). Low frequency oscillations are involved in attention processes and can modulate high-frequency oscillations, which can be abnormal in *Fmr1* KO mice (Radwan et al., 2016). Delta oscillations are primary contributors to the P3 wave of evoked responses to stimuli. Amplitude of P3 increases for stimuli that are unexpected or salient relative to background. Consistent with this notion, delta power is enhanced in attention deficit/hyperactivity disorder (ADHD), a comorbidity common in FXS (Hagerman and Hagerman, 2002). The *Fmr1* KO mice are also known to be hyperactive, and the enhanced delta power in AC and FC is only seen when the mice are moving (Fig. 4). Thus, the observed EEG abnormalities may be related to different symptoms in FXS, a notion that can be further tested if pharmacological approaches show correlated changes in specific EEG components and behavioral symptoms.

A potential mechanism for altered gamma oscillations is related to the function of parvalbumin positive (PV) interneurons. Multiple lines of evidence have shown that function of PV cells shapes normal gamma oscillations in the cortex (Cardin et al., 2009; Sohal et al., 2009; Carlen et al., 2012; Keeley et al., 2017) and that abnormal gamma power may arise from PV neuron dysfunctions (Lewis et al., 2005). Previous studies in the somatosensory cortex noted that the excitatory drive onto PV neurons was reduced in *Fmr1* KO mice (Selby et al., 2007; Gibson et al., 2008). Moreover, treatment of brain slices with chondroitinase ABC, an enzyme that removes chondroitin sulfate chains from perineuronal nets (PNN), was shown to reduce $GABA_A$ inhibitory postsynaptic currents (Liu et al., 2013) and reduce excitability of PV fast spiking cortical interneurons (Balmer, 2016). Data from our lab showed reduced formation of the PNNs around PV neurons in layers 2–4 in the auditory cortex of *Fmr1* KO mice at P21 (Wen et al., 2017). Impaired PNN development can lead to reduced excitability of cortical PV cells resulting in increased excitation of the network. Indeed, our studies demonstrate enhanced spontaneous and tone driven responses using single unit recordings in the developing auditory cortex of KO mice (Wen et al., 2017). Therefore, it is possible that altered gamma oscillations in the auditory cortex in FXS may arise from dysfunction of PV neurons and the abnormal development of PNNs that surround these interneurons. PNNs are regulated by matrix metalloprotease-9 (MMP-9), an enzyme that cleaves components of PNNs, such as aggrecan, fibronectin and laminin (D'ortho et al., 1997). MMP-9 levels are negatively regulated by FMRP (Janusz et al., 2013) and are elevated in FXS (Bilousova et al., 2009; Sidhu et al., 2014; Gkogkas et al., 2014). Genetic reduction or deletion of MMP-9 can alleviate symptoms in *Fmr1* KO mice (Sidhu et al., 2014; Lovelace et al., 2016; Wen et al., 2017), including impaired PNN formation around PV neurons and enhanced spontaneous and tone driven responses (Wen et al., 2017).

Future studies will utilize specific MMP-9 inhibitors to determine whether the EEG biomarkers described here and in humans will provide useful outcome measures in pre-clinical to clinical translation in FXS. We will also examine coupling of neural oscillations (Radwan et al., 2016) and utilize specific transgenic mouse lines in which FMRP is removed only from the forebrain and/or specific cell types to identify the mechanisms underlying altered neural oscillation dynamics in FXS. In conclusion, EEG recordings from the auditory and frontal cortex reveal multiple novel and translation-relevant phenotypes in the *Fmr1* KO mice with a strong potential to provide insight into mechanisms of sensory hypersensitivity and impaired sensory processing in FXS.

Acknowledgements

We thank members of the Ethell, Binder and Razak laboratories for helpful discussions. This work was supported by the National Institutes of Health (NIH) (1U54 HD082008-01 to IME, DKB and KAR), US Army Medical Research (W81XWH-15-1-0436 to IME, DKB and KAR) and FRAXA Research Foundation grant to JWL and KAR.

References

Abbeduto, L., Hagerman, R.J., 1997. Language and communication in fragile X syndrome. Dev. Disabil. Res. Rev. 3 (4), 313–322.
Abbeduto, L., Brady, N., Kover, S.T., 2007. Language development and fragile X syndrome: profiles, syndrome-specificity, and within-syndrome differences. Dev. Disabil. Res. Rev. 13 (1), 36–46.
Artieda, J., Valencia, M., Alegre, M., Olaziregi, O., Urrestarazu, E., Iriarte, J., 2004. Potentials evoked by chirp-modulated tones: a new technique to evaluate oscillatory activity in the auditory pathway. Clin. Neurophysiol. 115, 699–709.
Bakker, C.E., Verheij, C., Willemsen, R., Vanderhelm, R., Oerlemans, F., Vermey, M., Bygrave, A., Hoogeveen, A.T., Oostra, B.A., Reyniers, E., Deboulle, K., Dhooge, R., Cras, P., Vanvelzen, D., Nagels, G., Martin, J.J., Dedeyn, P.P., Darby, J.K., Willems, P.J., 1994. *Fmr1* knockout mice - a model to study fragile-x mental-retardation. Cell 78, 23–33.
Balmer, T.S., 2016. Perineuronal nets enhance the excitability of fast-spiking neurons. eNeuro 3 ENEURO-0112.
Bernardet, M., Crusio, W.E., 2006. Fmr1 KO mice as a possible model of autistic features. Sci. World J. 6, 1164–1176.
Berry-Kravis, E., 2002. Epilepsy in fragile X syndrome. Dev. Med. Child Neurol. 44, 724–728.
Berry-Kravis, E.M., Lindemann, L., Jønch, A.E., Apostol, G., Bear, M.F., Carpenter, R.L., Crawley, J.N., Curie, A., Des Portes, V., Hossain, F., Gasparini, F., 2018. Drug development for neurodevelopmental disorders: lessons learned from fragile X syndrome. Nat. Rev. Drug Discov. 17, 280–299.
Berzhanskaya, J., Phillips, M.A., Gorin, A., Lai, C., Shen, J., Colonnese, M.T., 2017. Disrupted cortical state regulation in a rat model of fragile X syndrome. Cereb. Cortex

27, 1386–1400.
Bilousova, T.V., Dansie, L., Ngo, M., Aye, J., Charles, J.R., Ethell, D.W., Ethell, I.M., 2009. Minocycline promotes dendritic spine maturation and improves behavioural performance in the fragile X mouse model. J. Med. Genet. 46, 94–102.
Cardin, J.A., Carlén, M., Meletis, K., Knoblich, U., Zhang, F., Deisseroth, K., Tsai, L.H., Moore, C.I., 2009. Driving fast-spiking cells induces gamma rhythm and controls sensory responses. Nature 459, 663.
Carlen, M., Meletis, K., Siegle, J.H., Cardin, J.A., Futai, K., Vierling-Claassen, D., Ruehlmann, C., Jones, S.R., Deisseroth, K., Sheng, M.I.M.C., Moore, C.I., 2012. A critical role for NMDA receptors in parvalbumin interneurons for gamma rhythm induction and behavior. Mol. Psychiatry 17, 537.
Castren, M., Paakkonen, A., Tarkka, I.M., Ryynanen, M., Partanen, J., 2003. Augmentation of auditory N1 in children with fragile X syndrome. Brain Topogr. 15, 165–171.
Crawford, D.C., Acuña, J.M., Sherman, S.L., 2001. FMR1 and the fragile X syndrome: human genome epidemiology review. Genet. Med. 3, 359–371.
D'ortho, M.P., Will, H., Atkinson, S., Butler, G., Messent, A., Gavrilovic, J., Smith, B., Timpl, R., Zardi, L., Murphy, G., 1997. Membrane-type matrix metalloproteinases 1 and 2 exhibit broad-spectrum proteolytic capacities comparable to many matrix metalloproteinases. FEBS J. 250, 751–757.
Dadarlat, M.C., Stryker, M.P., 2017. Locomotion enhances neural encoding of visual stimuli in mouse V1. J. Neurosci. 37, 3764–3775.
Dansie, L.E., Phommahaxay, K., Okusanya, A.G., Uwadia, J., Huang, M., Rotschafer, S.E., Razak, K.A., Ethell, D.W., Ethell, I.M., 2013. Long-lasting effects of minocycline on behavior in young but not adult Fragile X mice. Neuroscience 246, 186–198.
Darnell, J.C., Van Driesche, S.J., Zhang, C., Hung, K.Y.S., Mele, A., Fraser, C.E., Stone, E.F., Chen, C., Fak, J.J., Chi, S.W., Licatalosi, D.D., Richter, J.D., Darnell, R.B., 2011. FMRP stalls ribosomal translocation on mRNAs linked to synaptic function and autism. Cell 146, 247–261.
Ethridge, L.E., White, S.P., Mosconi, M.W., Wang, J., Byerly, M.J., Sweeney, J.A., 2016. Reduced habituation of auditory evoked potentials indicate cortical hyper-excitability in Fragile X Syndrome. Transl. Psychiatry 6, e787.
Ethridge, L.E., White, S.P., Mosconi, M.W., Wang, J., Pedapati, E.V., Erickson, C.A., Byerly, M.J., Sweeney, J.A., 2017. Neural synchronization deficits linked to cortical hyper-excitability and auditory hypersensitivity in fragile X syndrome. Mol. Autism 8, 22.
Gage, N.M., Siegel, B., Roberts, T.P., 2003. Cortical auditory system maturational abnormalities in children with autism disorder: an MEG investigation. Dev. Brain Res. 144, 201–209.
Gkogkas, C.G., Khoutorsky, A., Cao, R., Jafarnejad, S.M., Prager-Khoutorsky, M., Giannakas, N., Kaminari, A., Fragkouli, A., Nader, K., Price, T.J., Konicek, B.W., 2014. Pharmacogenetic inhibition of eIF4E-dependent Mmp9 mRNA translation reverses fragile X syndrome-like phenotypes. Cell Rep. 9, 1742–1755.
Gibson, J.R., Bartley, A.F., Hays, S.A., Huber, K.M., 2008. Imbalance of neocortical excitation and inhibition and altered UP states reflect network hyperexcitability in the mouse model of fragile X syndrome. J. Neurophysiol. 100, 2615–2626.
Hagerman, R.J., Hagerman, P.J., 2002. Fragile X Syndrome: Diagnosis, Treatment, and Research. Taylor & Francis US.
Hagerman, R.J., Berry-Kravis, E., Kaufmann, W.E., Ono, M.Y., Tartaglia, N., Lachiewicz, A., Kronk, R., Delahunty, C., Hessl, D., Visootskak, J., Picker, J., Gane, L., Tranfaglia, M., 2009. Advances in the treatment of fragile X syndrome. Pediatrics 123, 378–390.
Janusz, A., Miłek, J., Perycz, M., Pacini, L., Bagni, C., Kaczmarek, L., Dziembowska, M., 2013. The Fragile X mental retardation protein regulates matrix metalloproteinase 9 mRNA at synapses. J. Neurosci. 33, 18234–18241.
Keeley, S., Fenton, A.A., Rinzel, J., 2017. Modeling fast and slow gamma oscillations with interneurons of different subtype. J. Neurophysiol. 117, 950–965.
Lachaux, J.P., Rodrigues, E., Martinerie, J., Varela, F.J., 1999. Measuring phase synchrony in brain signals. Hum. Brain Mapp. 8, 194–208.
Lewis, D.A., Hashimoto, T., Volk, D.W., 2005. Cortical inhibitory neurons and schizophrenia. Nat. Rev. Neurosci. 6, 312.
Liu, H., Gao, P.F., Xu, H.W., Liu, M.M., Yu, T., Yao, J.P., Yin, Z.Q., 2013. Perineuronal nets increase inhibitory GABAergic currents during the critical period in rats. Int. J. Ophthalmol. 6, 120.
Lovelace, J.W., Wen, T.H., Reinhard, S., Hsu, M.S., Sidhu, H., Ethell, I.M., Binder, D.K., Razak, K.A., 2016. Matrix metalloproteinase-9 deletion rescues auditory evoked potential habituation deficit in a mouse model of Fragile X Syndrome. Neurobiol. Dis. 89, 126–135.
Maris, E., Oostenveld, R., 2007. Nonparametric statistical testing of EEG- and MEG-data. J. Neurosci. Methods 164, 177–190.
Miller, L.J., McIntosh, D.N., McGrath, J., Shyu, V., Lampe, M., Taylor, A.K., Tassone, F., Nietzel, K., Stackhouse, T., Hagerman, R.J., 1999. Electrodermal responses to sensory stimuli in individuals with fragile X syndrome. Am. J. Med. Genet. 83, 268–279.
Musumeci, S.A., Hagerman, R.J., Ferri, R., Bosco, P., Bernardina, B.D., Tassinari, C.A., de Sarro, G.B., Elia, M., 1999. Epilepsy and EEG findings in males with fragile X syndrome. Epilepsia 40, 1092–1099.
Niell, C.M., Stryker, M.P., 2010. Modulation of visual responses by behavioral state in mouse visual cortex. Neuron 65, 472–479.
Orekhova, E.V., Stroganova, T.A., Nygren, G., Tsetlin, M.M., Posikera, I.N., Gillberg, C., Elam, M., 2007. Excess of high frequency electroencephalogram oscillations in boys with autism. Biol. Psychiatry 62, 1022–1029.
Perez-Alcazar, M., Nicolas, M.J., Valencia, M., Alegre, M., Iriarte, J., Artieda, J., 2008. Chirp-evoked potentials in the awake and anesthetized rat. A procedure to assess changes in cortical oscillatory activity. Exp. Neurol. 210, 144–153.
Purcell, D.W., John, S.M., Schneider, B.A., Picton, T.W., 2004. Human temporal auditory acuity as assessed by envelope following responses. J. Acoust. Soc. Am. 116, 3581–3593.
Radwan, B., Dvorak, D., Fenton, A.A., 2016. Impaired cognitive discrimination and discoordination of coupled theta–gamma oscillations in Fmr1 knockout mice. Neurobiol. Dis. 88, 125–138.
Roberts, J.E., Hatton, D.D., Bailey, D.B., 2001. Development and behavior of male toddlers with fragile X syndrome. J. Early Intervention 24, 207–223.
Rotschafer, S.E., Razak, K., 2013. Altered auditory processing in a mouse model of fragile X syndrome. Brain Res. 1506, 12–24.
Rotschafer, S.E., Razak, K.A., 2014. Auditory processing in fragile X syndrome. Front. Cell. Neurosci. 8.
Sabaratnam, M., Vroegop, P.G., Gangadharan, S.K., 2001. Epilepsy and EEG findings in 18 males with fragile X syndrome. Seizure 10, 60–63.
Salinas, E., Sejnowski, T.J., 2001. Correlated neuronal activity and the flow of neural information. Nat. Rev. Neurosci. 2, 539–550.
Schneider, A., Leigh, M.J., Adams, P., Nanakul, R., Chechi, T., Olichney, J., Hagerman, R., Hessl, D., 2013. Electrocortical changes associated with minocycline treatment in fragile X syndrome. J. Psychopharmacol. 27, 956–963.
Selby, L., Zhang, C., Sun, Q.Q., 2007. Major defects in neocortical GABAergic inhibitory circuits in mice lacking the fragile X mental retardation protein. Neurosci. Lett. 412, 227–232.
Sidhu, H., Dansie, L.E., Hickmott, P.W., Ethell, D.W., Ethell, I.M., 2014. Genetic removal of matrix metalloproteinase 9 rescues the symptoms of fragile X syndrome in a mouse model. J. Neurosci. 34, 9867–9879.
Sinclair, D., Oranje, B., Razak, K.A., Siegel, S.J., Schmid, S., 2016. Sensory processing in autism spectrum disorders and Fragile X syndrome-from the clinic to animal models. Neurosci. Biobehav. Rev. 76, 235–253.
Sinclair, D., Featherstone, R., Naschek, M., Nam, J., Du, A., Wright, S., Pance, K., Melnychenko, O., Weger, R., Akuzawa, S., Matsumoto, M., Siegel, S.J., 2017. GABA-B agonist baclofen normalizes auditory-evoked neural oscillations and behavioral deficits in the Fmr1 knockout mouse model of fragile X syndrome. eNeuro 4 (1).
Sohal, V.S., Zhang, F., Yizhar, O., Deisseroth, K., 2009. Parvalbumin neurons and gamma rhythms enhance cortical circuit performance. Nature 459, 698.
Sørensen, E.M., Bertelsen, F., Weikop, P., Skovborg, M.M., Banke, T., Drasbek, K.R., Scheel-Krüger, J., 2015. Hyperactivity and lack of social discrimination in the adolescent Fmr1 knockout mouse. Behav. Pharmacol. 26, 733–740.
Stapells, D., 2011. Frequency-specific ABR and ASSR threshold assessment in young infants. In: Comprehensive Handbook of Pediatric Audiology. Plural Publishing, San Diego, pp. 409–448.
Stienen, P.J., Venzi, M., Poppendieck, W., Hoffmann, K.P., Aberg, E., 2016. Precaution for volume conduction in rodent cortical electroencephalography using high-density polyimide-based microelectrode arrays on the skull. J. Neurophysiol. 115, 1970–1977.
Tallon-Baudry, C., Bertrand, O., Delpuech, C., Pernier, J., 1996. Stimulus specificity of phase-locked and non-phase-locked 40 Hz visual responses in human. J. Neurosci. 16, 4240–4249.
Van der Molen, M.J.W., Van der Molen, M.W., 2013. Reduced alpha and exaggerated theta power during the resting-state EEG in fragile X syndrome. Biol. Psychol. 92, 216–219.
Van der Molen, M.J., Huizinga, M., Huizenga, H.M., Ridderinkhof, K.R., Van der Molen, M.W., Hamel, B.J., Curfs, L.M., Ramakers, G.J., 2010. Profiling fragile X syndrome in males: strengths and weaknesses in cognitive abilities. Res. Dev. Disabil. 31, 426–439.
Van der Molen, M.J.W., Van der Molen, M.W., Ridderinkhof, K.R., Hamel, B.C.J., Curfs, L.M.G., Ramakers, G.J.A., 2012a. Auditory change detection in fragile X syndrome males: a brain potential study. Clin. Neurophysiol. 123, 1309–1318.
Van der Molen, M.J.W., Van der Molen, M.W., Ridderinkhof, K.R., Hamel, B.C.J., Curfs, L.M.G., Ramakers, G.J.A., 2012b. Auditory and visual cortical activity during selective attention in fragile X syndrome: a cascade of processing deficiencies. Clin. Neurophysiol. 123, 720–729.
Vinck, M., Oostendveld, R., Van Wingerden, M., Barraglia, F., 2011. An improved index of phase-sychronization for elecrophysiological data in the presence of volume-doncutcion, noise, and sample-size bias. NeuroImage 55, 1548–1565.
Wang, J., Barstein, J., Ethridge, L.E., Mosconi, M.W., Takarae, Y., Sweeney, J.A., 2013. Resting state EEG abnormalities in autism spectrum disorders. J. Neurodev. Disord. 5, 24.
Wang, J., Ethridge, L.E., Mosconi, M.W., White, S.P., Binder, D.K., Pedapati, E.V., Erickson, C.A., Byerly, M.J., Sweeney, J.A., 2017. A resting EEG study of neocortical hyperexcitability and altered functional connectivity in fragile X syndrome. J. Neurodev. Disord. 9 (1), 11.
Wen, T.H., Afroz, S., Reinhard, S.E., Tapia, K., Binder, D.K., Razak, K.A., Ethell, I.M., 2017. Genetic reduction of matrix metalloproteinase-9 promotes formation of perineuronal nets around parvalbumin-expressing interneurons and normalizes auditory cortex responses in developing Fmr1 knock-out mice (2017). Cereb. Cortex. http://dx.doi.org/10.1093/cercor/bhx258.
Wisniewski, K.E., Segan, S.M., Miezejeski, C.M., Sersen, E.A., Rudelli, R.D., 1991. The Fra (X) syndrome: neurological, electrophysiological, and neuropathological abnormalities. Am. J. Med. Genet. 38, 476–480.
Yu, S., Pritchard, M., Kremer, E., Lynch, M., Nancarrow, J., Baker, E., Holman, K., Mulley, S., Warren, T., Schlessinger, D., Sutherland, G.R., Richards, R.I., 1991. Fragile X genotype characterized by an unstable region of DNA. Science 252, 1179–1181.